Cobalt Coordination Networks Based on the Linker (Phenazine-5,10-diyl)di- and Tetrabenzoate

Annette Vollrath, Xiang Liu, Nikolas Jansen, Philipp Seiffert, David Geller, Christoph Janiak

crystals

MDPI

Article

Cobalt Coordination Networks Based on the Linker (Phenazine-5,10-diyl)di- and Tetrabenzoate

Annette Vollrath, Xiang Liu, Nikolas Jansen, Philipp Seiffert, David Geller and Christoph Janiak *

Institut für Anorganische Chemie und Strukturchemie, Heinrich-Heine-Universität, 40204 Düsseldorf, Germany; annette.vollrath@hhu.de (A.V.); xiang.liu@hhu.de (X.L.); nijan113@hhu.de (N.J.); philipp.seiffert@hhu.de (P.S.); david.geller@hhu.de (D.G.)

* Correspondence: janiak@uni-duesseldorf.de

Abstract

The crystal structures of the cobalt(II) metal–organic frameworks or coordination networks of [Co(pdb)(DMF)] and $[Co_2(pdi)(DMF)_3]\cdot 2(DMF)\cdot H_2O$ (H_2pdb = 3,3′-(phenazine-5,10-diyl)dibenzoic acid; H_4pdi = 5,5′-(phenazine-5,10-diyl)diisophthalic acid; DMF = *N*,*N*-dimethylformamide) were synthesized solvothermally from cobalt(II) nitrate and the free acid of the linker in DMF. Systematic solvothermal screening demonstrated strong metal- and counterion-dependent framework formation, as crystalline coordination polymers were obtained exclusively from cobalt(II) nitrate, whereas other metal salts and cobalt(II) chloride or sulfate produced no crystalline materials. In catena-[(*N*,*N*-dimethylformamide)-μ_4-3,3′-(phenazine-5,10-diyl)dibenzoate-cobalt(II)], [Co(pdb)(DMF)], the Co_2 units, acting as secondary building units, are coordinated by four carboxylate groups from four linkers in a paddle-wheel arrangement, giving a three-dimensional (3D) network with cds (or $CdSO_4$) topology, in which the wide openings are filled by two symmetry-related nets to form a threefold interpenetrated structure. In catena-[tris(*N*,*N*-dimethylformamide)-μ_8-5,5′-(phenazine-5,10-diyl)diisophthalate-dicobalt(II)] bis(*N*,*N*-dimethylformamide) hydrate, $[Co_2(pdi)(DMF)_3]\cdot 2(DMF)\cdot H_2O$, there are two different Co atoms, of which only Co_2 is connected to each of the four carboxylate groups of the tetracarboxylate linker and, thus, is responsible for 3D network formation. The network topology in $[Co_2(pdi)(DMF)_3]$ is pts (or platinum(II) sulfide) when taking the Co_2 atom as a tetrahedral node and the linker as a square-planar fourfold node; however, this arrangement is inverse to the common square-planar metal and tetrahedral linker nodes found in PtS and most pts topologies.

Keywords: cobalt coordination networks; dihydrophenazine; 3-fold interpenetrated cds topology; inverse pts topology; redox-active linker

Academic Editor: Peter Baran

Received: 15 January 2026
Revised: 1 March 2026
Accepted: 2 March 2026
Published: 10 March 2026

1. Introduction

Incorporating redox-active carboxylate linkers—such as those based on phenazine—into the construction of new coordination polymers (CPs) and metal–organic frameworks (MOFs) offers expanded opportunities to harness redox behavior [1–4]. Phenazine derivatives contain a dibenzo-fused pyrazine core and are well known for their intrinsic redox activity. They can be readily reduced to 5,10-dihydrophenazines, which, together with subsequent transformations, give access to a wide range of dihydrophenazine derivatives (Scheme 1) [5]. Dihydrophenazines (DHPs), particularly *N*,*N*′-substituted diaryl-phenazin-5,10-diyls, are electron-rich species that generate stable radical cations upon irradiation, heating, electrochemical oxidation, or treatment with suitable chemical oxidants [6]. Owing to their pronounced

redox activity and the stability of their radical cations [7,8], DHPs display distinctive optical, electronic, magnetic, and catalytic characteristics [9–11]. Several diaryl-substituted DHPs have been identified as effective photoredox catalysts for visible light-mediated atom transfer radical polymerization [12–17].

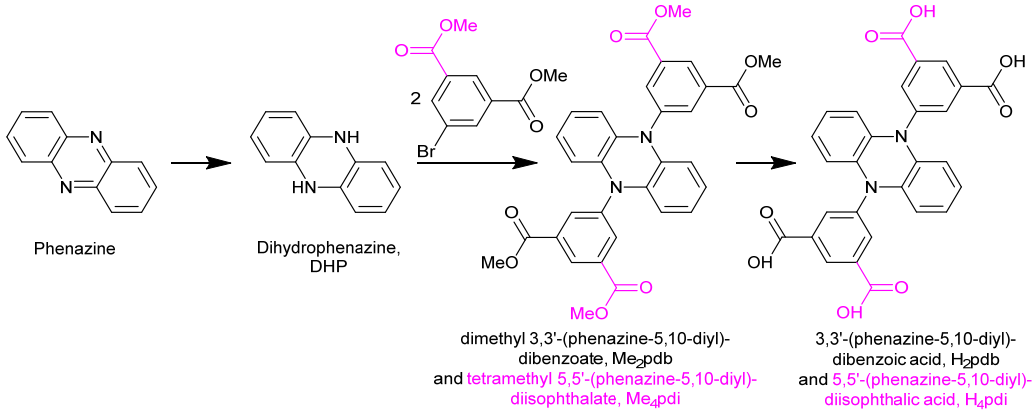

Scheme 1. Synthesis route to the free acids of the H_2pdb = 3,3′-(phenazine-5,10-diyl)dibenzoic acid (black skeletons) and H_4pdi = 5,5′-(phenazine-5,10-diyl)diisophthalic acid (black plus pink structure parts; the attached methylcarboxyl and carboxyl groups in pink are only present in the Me_4pdi and H_4pdi compounds). For details, see Section 2 and Section S2 in the Supplementary Materials.

Dihydrophenazine-based organic polymers [9,10,18], MOFs [10,19,20] and coordination cages [21] have been investigated for their electrochemical behavior [22–24] and have been explored as heterogeneous catalysts. While previous publications have reported on phenazine-based covalent organic frameworks (COFs) used for catalytic and optoelectronic applications [25–27], DHP-containing 2D and 3D covalent organic frameworks have demonstrated high efficiency as heterogeneous photocatalysts for the radical ring-opening polymerization of vinylcyclopropanes [18]. UiO-type MOF $[Zr_6(\mu_3\text{-}O)_4(\mu_3\text{-}OH)_4(pzdb)_6]$ (pzdb = 4,4′-(phenazine-5,10-diyl)dibenzoate)) [10] has been successfully utilized as a heterogeneous donor component to enhance catalytic electron donor–acceptor photoactivation. Similarly, the $[Zn_2(pzdb)_2(dabco)]\cdot 4DMF$ (dabco = 1,4-diazabicyclo[2.2.2]octane) framework has been applied as a heterogeneous catalyst for aza-Diels–Alder reactions [28].

Recently, UV/Vis/NIR spectroelectrochemistry revealed that the pzdb linker is the primary redox site in coordination polymers $[Zn(pzdb)(DEF)_2]$ and $[Co(Hpzdp)_2(DEF)_2]$ (DEF = *N*,*N*-diethylformamide) upon electrochemical oxidation or chemical oxidation with $SbCl_5$ based on the same color changes as in Me_2pzdb, together with EPR signals typical of ligand-based radical cations. However, the coordination polymers decomposed upon pzdb linker oxidation [29].

Here, we report the synthesis and characterization of two new coordination networks based on DHP-derived redox-active linkers H_2pdb and H_4pdi.

2. Materials and Methods

All chemicals were purchased from commercial suppliers and used without further purification (see Supplementary Material, Section S1 for details). Deionized water was employed in all procedures involving water using a Sartorius Arium Mini water purifier (Sartorius, Göttingen, Germany). Single-crystal X-ray diffraction data were collected on a Rigaku XtaLAB Synergy S instrument (Rigaku, Tokyo, Japan) equipped with a PhotonJet Cu Kα radiation source (λ = 1.54184 Å) and a hybrid pixel array detector. Suitable crystals were selected under a Leica M80 polarized-light microscope (Leica, Wetzlar, Germany) and mounted on a cryo-loop in oil. Data processing—including unit-cell refinement, data reduction, and absorption correction—was carried out with CrysAlisPro, version

171.42.102a. Structures were solved and refined in Olex2, version 1.5, using SHELXT and SHELXL, respectively [30–32]. Molecular graphics were generated using Diamond 5 software [33].

Powder X-ray diffraction (PXRD) data were collected at room temperature on a Rigaku Mini-Flex600 diffractometer (Rigaku, Tokyo, Japan) (600 W, 40 kV, 15 mA) using Cu Kα radiation (λ = 1.54184 Å). The samples were dried for 12 h at 60 °C under vacuum. PXRD patterns were normalized to the intensity of the most intense peak. Simulated PXRD patterns were obtained from MERCURY 2020.3.0 using the single-crystal XRD data [34].

Fourier transform infrared (FT-IR) spectra were recorded between 500 and 4000 cm^{-1} using a Bruker TENSOR 37 spectrometer (Bruker, Billerica, MA, USA) in ATR mode (Platinum ATR-QL, Diamond). Nuclear magnetic resonance (NMR) spectra were measured on a Bruker Avance III 300 spectrometer (Bruker, Billerica, MA, USA) operating at 300 MHz for ^{1}H NMR and 150 MHz for ^{13}C NMR. Electron impact (EI) mass spectra were obtained using a Thermo Finnigan Trace DSQ spectrometer (Thermo Fisher Scientific, Waltham, MA, USA).

N_2 sorption measurements were carried out with a Belsorp Max II (Microtrac, MRB, Haan, Germany) volumetric gas sorption analyzer at 77 K. Samples were pre-dried for 12 h at 60 °C under vacuum, then activated at the sorption analyzer under turbomolecular pump vacuum ($5 \cdot 10^{-12}$ bar) for 3 h at 130 °C.

Thermogravimetric analysis (TGA) was carried out in air and under nitrogen on a Netzsch TG209 F3 Tarsus instrument (Netzsch, Selb, Germany) at a heating rate of 10 K min^{-1} up to 1000 °C. Gaseous products were analyzed with a GAM 200 mass spectrometer from InProcess Instruments (InProcess Instruments, Bremen, Germany). Melting points were measured in open capillaries using a Büchi Melting Point B-540 apparatus (Büchi Labortechnik AG, Flawil, Switzerland).

Elemental analyses were conducted on a PerkinElmer 2400 series II elemental analyzer (PerkinElmer, Waltham, MA, USA) (accuracy of 0.5%). The samples were dried at 180 °C under vacuum (10^{-3} bar).

Electrochemical experiments were performed using an Interfere 1010E potentiostat (Gamry Instruments, Warminster, PA, USA) coupled with an RRDE-3A system (ALS, Tokyo, Japan). Measurements were carried out in a three-electrode configuration, employing an Ag/AgCl reference electrode (stored in 3.5 mol L^{-1} KCl), a platinum counter electrode, and a glassy carbon working electrode with a diameter of 5 mm. The electrolyte consisted of nitrogen-purged acetonitrile containing 0.5 mol L^{-1} tetrabutylammonium hexafluorophosphate. The catalyst ink was prepared by dispersing 1 mg of the sample in a mixture of 0.25 mL of ethanol and 0.25 mL of water, followed by sonication for 30 min. Subsequently, 10 µL of the ink was drop-cast onto the working electrode and dried at 150 rpm, resulting in a catalyst loading of approximately 10 µg cm^{-2}. Cyclic voltammetry measurements were conducted over a potential range of −0.7 V to 1.5 V versus Ag/AgCl at a scan rate of 100 mV s^{-1}.

2.1. Synthesis of 5,10-Dihydrophenazine (Scheme S1)

Phenazine (4.00 g, 22.2 mmol) was dissolved in 50 mL of ethanol in a 500 mL round-bottom flask. Sodium dithionite (38.7 g, 222 mmol) was dissolved in 250 mL of deionized water. The two solutions were then combined in the flask, which was heated to 95 °C under stirring and reflux for 3 h. After the flask was cooled to room temperature. the reaction mixture was filtered, and the product was dried under vacuum for 40 min. Finally, the product was stored under a protective N_2 atmosphere. Yield: 3.69 g (91%). ^{1}H-NMR (300 MHz, DMSO-d_6): δ [ppm] = 7.29 (s, 2 H), 6.25 (dd, J = 6.7, 3.4 Hz, 4 H), 6.01 (dd, J = 6.7, 3.5 Hz, 4 H).

2.2. Synthesis of Dimethyl-3,3′-(Phenazine-5,10-diyl)Dibenzoate (Me_2pdb) (Scheme S2)

A 100 mL three-neck flask was charged with 1.00 g of 5,10-dihydrophenazine (5.50 mmol), 2.60 g of 3-methyl 3-bromobenzoate (12.1 mmol), and 1.52 g of potassium carbonate (16.5 mmol). After sealing the flask, a solution of 0.062 g of palladium(II)-acetate (0.27 mmol) and 0.3 mL of tri-*tert*-butylphosphine dissolved in 60 mL of xylene was added. The reaction mixture was heated under stirring to reflux for 48 h. After cooling to room temperature, 100 mL of water was added to the reaction mixture, and it was extracted with 3 × 150 mL of dichlormethane. The combined organic phases were washed with 150 mL of brine solution (60 g NaCl in 300 mL water) and were dried over magnesium sulfate. The organic solution was concentrated using a rotary evaporator. After adding 5 mL of DCM and 40 mL of n-hexane, the product was recrystallized in the refrigerator. The precipitate was filtered off and dried under vacuum. Yield: 1.83 g (74%). ^{1}H-NMR (300 MHz, $CDCl_3$): δ [ppm] = 8.20–8.08 (m, 4 H), 7.71 (t, J = 9.0, 6.0 Hz, 2 H), 7.65–7.59 (m, 4 H), 6.28 (dd, J = 6.7, 3.4 Hz, 4 H), 5.58 (dd, J = 6.7, 3.4 Hz, 4 H), 3.94 (s, 6 H). %). ^{13}C{^{1}H}-NMR (600 MHz, $CDCl_3$): δ [ppm] = 166.16, 140.34, 136.31, 136.16, 133.73, 132.93, 131.51, 129.49, 121.13, 112.62, 52.36. [HR-ESI-MS] m/z = 450.16 (calculated for $^{12}C_{28}$ $^{1}H_{22}$ $^{14}N_2$ $^{16}O_4$ 450.16). IR (ATR): υ [cm^{-1}] = 3430, 3076, 3037, 3006, 2953, 2841, 2625, 2579, 1911, 1719, 1660, 1629, 1609, 1596, 1580, 1484, 1440, 1391, 1347, 1287, 1261, 1192, 1173, 1158, 1129, 1098, 1078, 1062, 991, 949, 928, 889, 838, 813, 794, 733, 693, 678, 643, 618, 558. Mp. = 255 °C.

2.3. Synthesis of 3,3′-(Phenazine-5,10-diyl)Dibenzoic Acid (H_2pdb) (Scheme S3)

A solution of 1.72 g (3.82 mmol) of dimethyl-3,3′-(phenazine-5,10-diyl)dibenzoate in 25 mL of 1,4-dioxane was prepared in a 100 mL flask. Then, 1.60 g of lithium hydroxide (38.2 mmol) and 15 mL of water were added to the reaction mixture, which was then heated to 100 °C for 24 h. After cooling to room temperature, the mixture was neutralized with concentrated hydrochloric acid (~1.9 mL). The precipitation was then filtered and dried under vacuum. Yield: 1.53 g (91%). ^{1}H-NMR (300 MHz, DMSO-d_6): δ [ppm] = 13.07 (s, 2 H), 8.08 (dt, 2 H), 7.92 (t, J = 9.0, 6.0 Hz, 2 H), 7.82 (t, J = 9.0, 6.0 Hz, 2 H), 7,73 (dt, 2 H), 6.30 (dd, J = 6.7, 3.4 Hz, 4 H), 5.52 (dd, J = 6.7, 3.4 Hz, 4 H). ^{13}C{^{1}H}-NMR (600 MHz, DMSO-d_6): δ [ppm] = 166.47, 139.94, 135.75, 134.75, 134.74, 132.00, 131.70, 129.25, 121.19, 112.49. [HR-ESI-MS] m/z = 422.13 (calculated for $^{12}C_{26}$ $^{1}H_{18}$ $^{14}N_2$ $^{16}O_4$ 422.13). IR (ATR): υ [cm^{-1}] = 3386, 3067, 2994, 2857, 2814, 2662, 2540, 1979, 1909, 1865, 1821, 1748, 1683, 1609, 1597, 1581, 1483, 1443, 1411, 1388, 1344, 1280, 1183, 1160, 1138, 1103, 1082, 1061, 1002, 990, 965, 928, 912, 838, 819, 757, 734, 693, 669, 643, 617, 568. Mp. > 350 °C.

2.4. Synthesis of Tetramethyl-5,5′-(Phenazine-5,10-diyl)Diisophthalate (Me_4pdi) (Scheme S4)

A 100 mL three-neck flask was charged with 1.00 g of 5,10-dihydrophenazine (5.50 mmol), 2.60 g of dimethyl-5-bromoisophthalate (12.1 mmol), and 1.52 g of potassium carbonate (16.5 mmol). After sealing the flask, a solution of 0.062 g of palladium(II)-acetate (0.27 mmol) and 0.3 mL of tri-*tert*-butylphosphine dissolved in 60 mL of xylene was added. The reaction mixture was heated under stirring to reflux for 48 h. After cooling to room temperature, 100 mL of water was added to the reaction mixture, and it was extracted with 3 × 150 mL of dichlormethane. The combined organic phases were washed with 150 mL of brine solution (60 g NaCl in 300 mL water) and were dried over magnesium sulfate. The organic solution was concentrated using a rotary evaporator. After adding 5 mL of DCM and 40 mL of *n*-hexane, the product was recrystallized in a refrigerator. The precipitate was filtered off and dried under vacuum. Yield: 2.12 g (68%). ^{1}H-NMR (300 MHz, $CDCl_3$): δ [ppm] = 8.80 (t, J = 3.0, 3.0 Hz, 2 H), 8.32 (d, 4 H), 6.32 (dd, J = 6.7, 3.4 Hz, 4 H), 5.59 (dd, J = 6.7, 3.4 Hz, 4 H), 3.98 (s, 12 H). ^{13}C{^{1}H}-NMR (600 MHz, $CDCl_3$): δ [ppm] = 165.47, 141.00, 137.72, 135.96, 134.35, 130.68, 121.66, 113.12, 52.79. [HR-ESI-MS] m/z = 566.17

(calculated for $^{12}C_{32}$ $^{1}H_{26}$ $^{14}N_2$ $^{16}O_8$ 566.17). IR (ATR): υ [cm^{-1}] = 3431, 3088, 3004, 2954, 2846, 1718, 1590, 1544, 1489, 1434, 1398, 1355, 1307, 1287, 1242, 1199, 1167, 1137, 1105, 1065, 998, 950, 938, 918, 898, 876, 834, 806, 784, 753, 741, 723, 686, 664, 618, 562. Mp. = 336 °C.

2.5. Synthesis of 5,5′-(Phenazine-5,10-diyl)Diisophthalic Acid (H_4pdi) (Scheme S5)

A solution of 1.00 g (1.77 mmol) of tetramethyl-5,5′-(phenazine-5,10-diyl)diisophthalate in 25 mL of 1,4-dioxane was prepared in a 100 mL flask. Then, 0.74 g of lithium hydroxide (17.7 mmol) and 15 mL of water were added to the reaction mixture, which was heated to 100 °C for 24 h. After cooling to room temperature, the mixture was neutralized with concentrated hydrochloric acid (~1.5 mL). The precipitation was then filtered and dried under vacuum. Yield: 0.71 g (79%). ^{1}H-NMR (300 MHz, D_2O): δ [ppm] = 8.33 (t, J = 3.0, 3.0 Hz, 2 H), 7.89 (d, 4 H), 6.30 (dd, J = 6.7, 3.4 Hz, 4 H), 5.67 (dd, J = 6.7, 3.4 Hz, 4 H). ^{13}C{^{1}H}-NMR (600 MHz, D_2O): δ [ppm] = 174.03, 140.06, 139.67, 136.08, 134.08, 128.94, 121.48, 113.00. IR (ATR): υ [cm^{-1}] = 3384, 3079, 3063, 2981, 2861, 2824, 2665, 2616, 2572, 2540, 1891, 1865, 1723, 1694, 1635, 1591, 1552, 1488, 1455, 1423, 1351, 1311, 1279, 1244, 1192, 1159, 1109, 1064, 1003, 957, 925, 847, 790, 756, 729, 693, 681, 661, 615, 602. Mp. > 350 °C.

2.6. Synthesis of Catena-[(N,N-Dimethylformamide)-μ_4-3,3′-(Phenazine-5,10-diyl)Dibenzoate-Cobalt(II)], [Co(pdb)(DMF)]

First, 15.0 mg of H_2pdb (0.034 mmol) and 20.0 mg of cobalt nitrate hexahydrate (0.068 mmol) were placed in a glass tube. Then, 2 mL of DMF was added to completely dissolve the solids. The tubes were sealed and placed in an oven at 100 °C for two days. Dark-red crystals were obtained as a final product. The crystals were washed with DMF and ethanol and dried under vacuum. Yield: 11 mg (56%). $C_{29}H_{23}CoN_3O_5$ ([Co(pdb)(DMF)]): calc. C C 63.04, H 4.20, N 7.61%; exp. C 62.14, H 4.23, N 7.76%.

MOFs and coordination networks cannot be purified by recrystallization as molecular compounds can. Importantly, varying degrees of missing linker or missing cluster defects lead to deviations from the ideal formula, which cannot be alleviated. A missing anionic linker cannot only be replaced by coordinated solvent but also needs hydroxide or anionic ligands from the metal salt precursor for charge compensation. Furthermore, a difficult-to-control loss of crystal or coordinating solvent molecules and possible hydration upon sample handling in air can also occur. Therefore, elemental analyses are often not reported for MOFs because of the known mismatch. Crystal-phase purity is usually established by matching the experimental and simulated PXRD.

2.7. Synthesis of Catena-[tris(N,N-Dimethylformamide)-μ_8-5,5′-(Phenazine-5,10-diyl)Diisophthalate-Dicobalt(II)] bis(N,N-Dimethylformamide) Hydrate $[Co_2(pdi)(DMF)_3]\cdot 2(DMF)\cdot H_2O$

First, 17.9 mg of H_4pdi (0.035 mmol) and 20 mg of cobalt nitrate hexahydrate (0.070 mmol) were placed in a glass tube. Then, 2 mL of DMF was added to completely dissolve the solids. The tubes were sealed and placed in an oven at 100 °C for two days. Dark-red crystals were obtained as a final product. The crystals were washed with DMF and ethanol and dried under vacuum. Yield: 22 mg (62%). $C_{43}H_{51}Co_2N_7O_{14}$ ($[Co_2(pdi)(DMF)_3]\cdot 2(DMF)\cdot H_2O$): calc. C C 51.24, H 5.10, N 9.73%; exp. C 48.56, H 3.58, N 6.73%. We note that for porous MOFs, the solvent content in the pores can change during sample handling, often leading to deviating elemental analyses (see also the comment on CHN analysis in Section 2.6).

3. Results and Discussion

The syntheses of the linkers started with the reduction of phenazine with sodium dithionate to 5,10-dihydrophenazine (DHP, Scheme 1, Scheme S1) [1]. DHP is a light-green solid and was stored under a nitrogen atmosphere because of its easy re-oxidation in air. ^{1}H NMR spectroscopy (Figure S1) confirmed the product with high purity. In the next reaction step, dimethyl-3,3′-(phenazine-5,10-diyl)dibenzoate [3,3′-(phenazine-5,10-diyl)dibenzoate dimethyl ester] or tetramethyl-5,5′-(phenazine-5,10-diyl)diisophthalate was synthesized (Schemes S2 or S4) through Buchwald–Hartwig coupling [19,35,36]. The highest yields and purest products were obtained with palladium(II) acetate as the catalyst, tri-*tert*-butylphosphine as the ligand and potassium carbonate as the base. The products are yellow or red powders, and their constitution and high purity are confirmed by NMR spectroscopy (Figures S2–S5).

Finally, the methyl esters were hydrolyzed with LiOH in a 1,4-dioxane/H_2O mixture to give 3,3′-(phenazine-5,10-diyl)dibenzoic acid as a light-yellow solid (H_2pdb, Scheme S3) or 5,5′-(phenazine-5,10-diyl)diisophthalic acid as a dark-green solid (H_4pdi, Scheme S5). Again the ^{1}H-NMR spectra are consistent with the constitutions (Figures S6–S9). The bands in the infrared spectra of the esters and the free acids can be assigned (Figures S10 and S11).

Various futile synthesis attempts were performed with zirconium(IV) chloride, zirconium oxychloride octahydrate, aluminum chloride hexahydrate, copper(II) chloride monohydrate, nickel(II) sulfate hexahydrate and nickel(II) chloride hexahydrate, with H_2pdb and H_4pdi in *N*,*N*-dimethylformamide giving no or no crystalline products. This was evident from the fact that either no reflections were visible in the measured PXRD (amorphous solid) or the same reflections as the pure linker were visible. Needle-shaped crystals from zinc nitrate hexahydrate with H_2pdb in a molar ratio of 1:3 at 120 °C after two days were too small for single-crystal X-ray diffractometry. Good-quality crystals were obtained only in the reactions of cobalt(II) nitrate hexahydrate with H_2pdb and H_4pdi (both with a 2:1 molar ratio at 100 °C) after two days (Figures S12 and S13). The anion plays a certain role, as identical reactions of cobalt(II) sulfate heptahydrate and cobalt(II) chloride hexahydrate yielded no solid products.

The experimental powder X-ray diffraction patterns of the bulk crystallized cobalt compounds matched well with the simulated patterns derived from the crystal structures of [Co(pdb)(DMF)] and $[Co_2(pdi)(DMF)_3]\cdot 2(DMF)\cdot H_2O$, confirming their phase purity (Section S5, Figures S15 and S16).

3.1. Crystal Structures of [Co(pdb)(DMF)]

Figure 1 shows the extended asymmetric unit and cobalt coordination environment of [Co(pdb)(DMF)], and Table 1 lists the crystallographic data. The space group of this compound is I2/a. It belongs to the monoclinic crystal system, and the asymmetric unit consists of one cobalt(II) ion, two half pdb linkers and a DMF ligand. The pdb linker with N1 has a twofold rotation axis passing through the phenazine core perpendicular to the ring plane. The linker with N3 has an inversion center at the centroid of the phenazine ring. The cobalt(II) ion is square-pyramidally surrounded by five oxygen atoms and forms a Co_2 handle as the secondary building unit (SBU) with another symmetry-equivalent cobalt(II) ion. This Co_2 handle is surrounded by four carboxylate groups from four linkers in a paddle-wheel arrangement. Each pdb ligand acts as a tetradentate bridging ligand and connects two Co_2 handles, being thereby bound to four cobalt atoms. The axial directions of the paddle-wheel unit bind to the oxygen atoms of the monodentate DMF ligands.

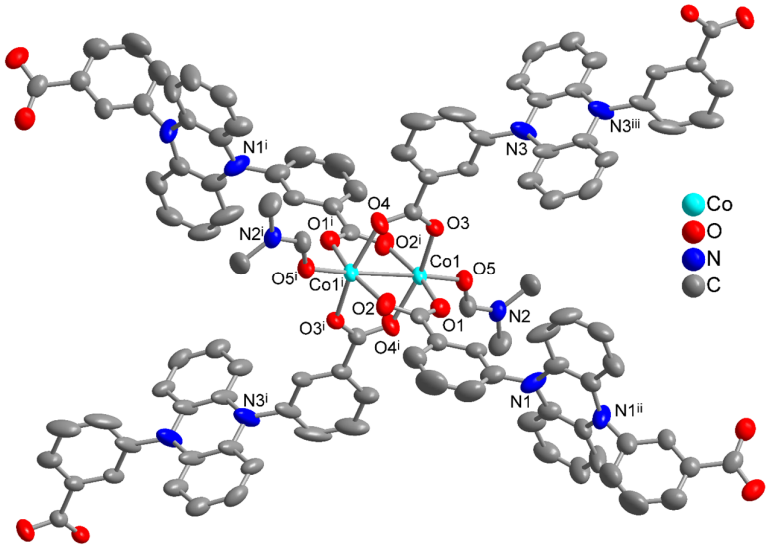

Figure 1. Expanded asymmetric unit for [Co(pdb)(DMF)]. Symmetry code: (i) −x + 1/2, −y + 3/2, −z + 3/2; (ii) −x + 3/2, y, −z + 1; (iii) −x, −y + 1, −z + 1 (50% thermal ellipsoids). Hydrogen atoms are not shown for clarity.

Table 1. Crystal data for [Co(pdb)(DMF)] and $[Co_2(pdi)(DMF)_3]\cdot 2(DMF)\cdot H_2O$.

	[Co(pdb)(DMF)]	**$[Co_2(pdi)(DMF)_3]\cdot 2(DMF)\cdot H_2O$**
empirical formula	$C_{29}H_{23}CoN_3O_5$	$C_{43}H_{51}Co_2N_7O_{14}$
mol wt (g mol^{-1})	552.43	1007.76
temperature (K)	150	150
crystal system	monoclinic	orthorhombic
space group	*I*2/a	*Pna*2_1
a (Å)	9.5099 (6)	26.9491 (5)
b (Å)	18.7609 (15)	15.5325 (3)
c (Å)	27.3129 (19)	11.4627 (2)
α (deg)	90	90
β (deg)	91.587 (6)	90
γ (deg)	90	90
volume, V ($Å^3$)	4871.1 (6)	4798.14 (15)
Z, Z′	8, 1	4, 1
D_{calc} (g/cm^3)	1.507	1.395
μ (mm^{-1})	5.922	6.02
F(000)	2280	2096
crystal size [mm^3]	0.09 × 0.05 × 0.04	0.1 × 0.07 × 0.05
wavelength (Å)	1.54184	1.54184
No. of unique reflections	4840	8579
No. of total reflections	27,266	64,849
No. of parameters	349	608

Table 1. *Cont.*

	[Co(pdb)(DMF)]	$[Co_2(pdi)(DMF)_3]\cdot 2(DMF)\cdot H_2O$
R_{int}	0.1268	0.0715
$R[F^2 > 2\sigma(F^2)]$ [a]	0.0632	0.0445
$wR[F^2 > 2\sigma(F^2)]$ [a]	0.1270	0.1091
R, $wR(F^2)$ [all data] [a]	0.1248, 0.1523	0.0494, 0.1116
S [all data] [a]	1.073	1.041
$\Delta\rho_{max}$, $\Delta\rho_{min}$ ($e\cdot Å^{-3}$) [b]	0.678, −0.471	0.722, −0.365
CCDC No.	2522790	2522791

[a] $R = [\Sigma(||F_o| - |F_c||)/\Sigma|F_o|]$; $wR = [\Sigma[w(F_o^2 - F_c^2)^2]/\Sigma[w(F_o^2)^2]]^{1/2}$. Goodness-of-fit $S = [\Sigma[w(F_o^2 - F_c^2)^2]/(n - p)]^{1/2}$. [b] Largest difference peak and hole.

The selected bond lengths and bond angles can be found in Table 2. The bond lengths of the four cobalt–oxygen bonds in the equatorial plane range from 2.00 Å to 2.09 Å, and the bond length of the cobalt–oxygen(DMF) bond in the axial direction is approximately 2.03 Å. The cobalt–cobalt distance in the Co_2 handle is 2.81 Å. The O-Co-O bond angles between the cis-positioned O atoms of the pdb linkers in the paddle-wheel unit are all approximately 90°, while the trans-O-Co-O angles are significantly smaller (~164°) because the Co···Co separation (2.81 Å) is larger than the O···O separation (~2.23 Å) in a carboxyl group so that the Co atom is placed "above" the equatorial plane of the four oxygen atoms. Consequently, the O-Co-O5(DMF) bond angle is also significantly greater than 90°. There is no significant π–π interaction and only limited C-H···π and C–H···O interactions in the supramolecular packing of the adjacent networks in [Co(pdb)(DMF)] (see Section S9 for details).

Table 2. Selected bond lengths (Å) and angles (°) for [Co(pdb)(DMF)] [a].

Interaction	Bond Length [Å]	Interaction	Angle [°]
Co1—O1	2.006 (4)	O1—Co1—O5	98.90 (15)
Co1—O2 ^{i}	2.023 (4)	O1—Co1—O2 ^{i}	163.69 (16)
Co1—O3	2.023 (3)	O2 ^{i}—Co1—O4 ^{i}	89.53 (15)
Co1—O4 ^{i}	2.081 (3)	O2 ^{i}—Co1—O5	97.18 (15)
Co1—O5	2.027 (3)	O3—Co1—O4 ^{i}	163.52 (13)
Co1···Co1 ^{i}	2.8068 (14)	O3—Co1—O5	100.55 (13)
		O3—Co1—O2 ^{i}	89.66 (13)
O1—Co1—O3	90.06 (13)	O5—Co1—O4 ^{i}	95.88 (13)
O1—Co1—O4 ^{i}	86.15 (14)		

[a] Symmetry code: i = −x + 1/2, −y + 3/2, −z + 3/2.

The Co_2 handles or SBUs are then linked into a three-dimensional network with cds topology (Figure 2). In cds (or $CdSO_4$) topology [37–40], each SBU is connected to four neighboring nodes via the linkers. If one starts with the chain shown in Figure 2a, where alternatingly, each SBU connects to a parallel chain from top to bottom and front to back, then the 3D network in Figure 2b is obtained.

The single network has wide openings that are several Ångströms across (Figure S13), even taking into account the space-filling van der Waals surface (Figure 2c). These openings are filled with two symmetry-related nets through interpenetration, giving a threefold interpenetrated structure with cds topology (Figure 3). Consequently,

no voids remain, and there is no porosity in the network. A threefold interpenetrated cds topology was described in 3D-[Co(pam)(bpa)(H_2O)$_2$]·DMF (H_2pam = pamoic acid, bpa = 1,2-di(4-pyridyl)ethylene, DMF = *N*,*N*-dimethylformamide) [41], and twofold interpenetrated cds net topologies were found in [Zn_2(BDC)(BPP)Cl_2] (BDC = benzene-1,4-dicarboxylate, BPP = 1,3-bis(4-pyridyl)propane) [42] and in [Cu(ceb)(bpmp)]·H_2O (ceb = 4-(carboxylatoethyl)benzoato, bpmp = 1,4-bis(pyridin-4-ylmethyl)piperazine) [43]. Further examples of interpenetrated networks with a cds topology are [Zn(Br-1,3-bdc)(NI-mbpy-34)] (Br-1,3-bdc = 5-bromobenzene-1,3-dicarboxylate, NI-mbpy-34 = *N*-(pyridin-3-ylmethyl)-4-(pyridin-4-yl)-1,8-naphthalimide) [44] and [M(μ-TBG)(μ-H_2O)(H_2O)$_2$]·2H_2O (M = Cu, Co and H_2TBG = terephthaloylbisglycine) [45]. A non-interpenetrated 3D network with cds topology was reported for [trans-Ni(H_2O)$_2$(μ-4,4′-bpy)$_2$](ClO_4)$_2$ (4,4′-bpy = 4,4′-bipyridine) [46].

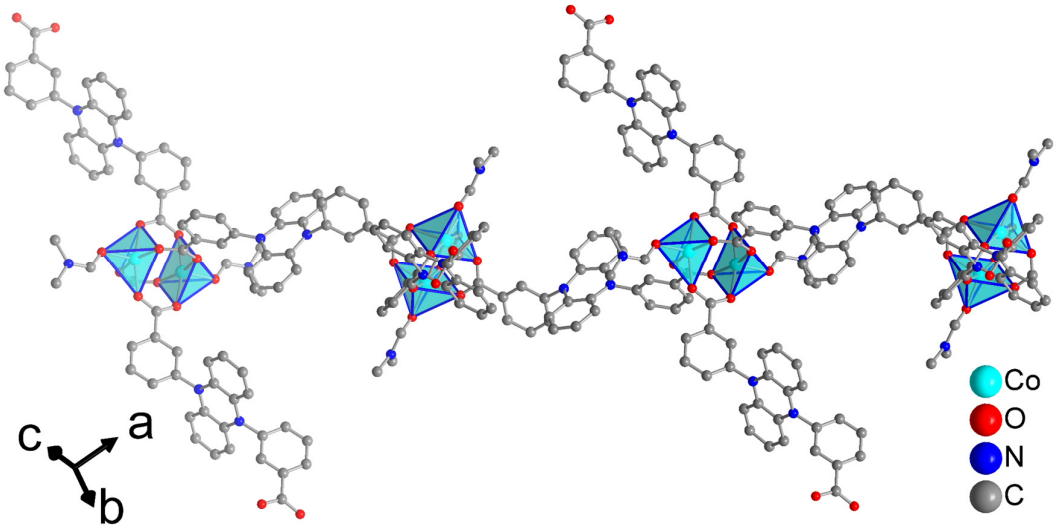

(**a**)

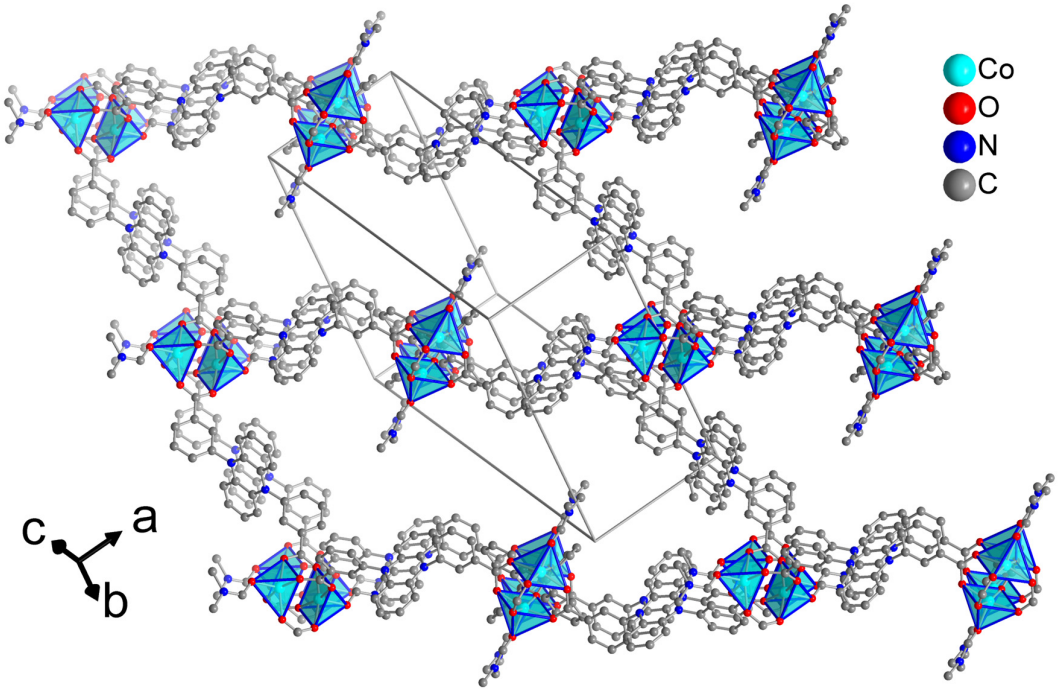

(**b**)

Figure 2. *Cont.*

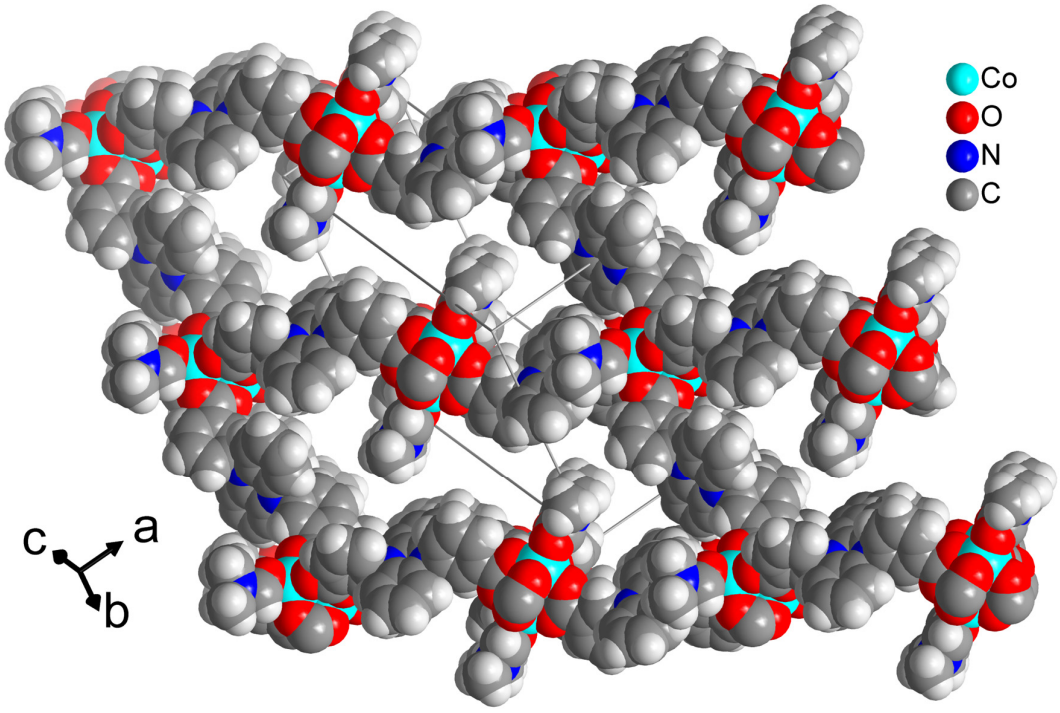

(**c**)

Figure 2. (**a**) Chain section of the 3D network in [Co(pdb)(DMF)], which is linked to parallel chains from top to bottom and front to back to give the full 3D network in (**b**) with cds topology. Hydrogen atoms are not shown for clarity, and the Co coordination is presented as polyhedra. (**c**) Space-filling view of the network with hydrogen atoms included.

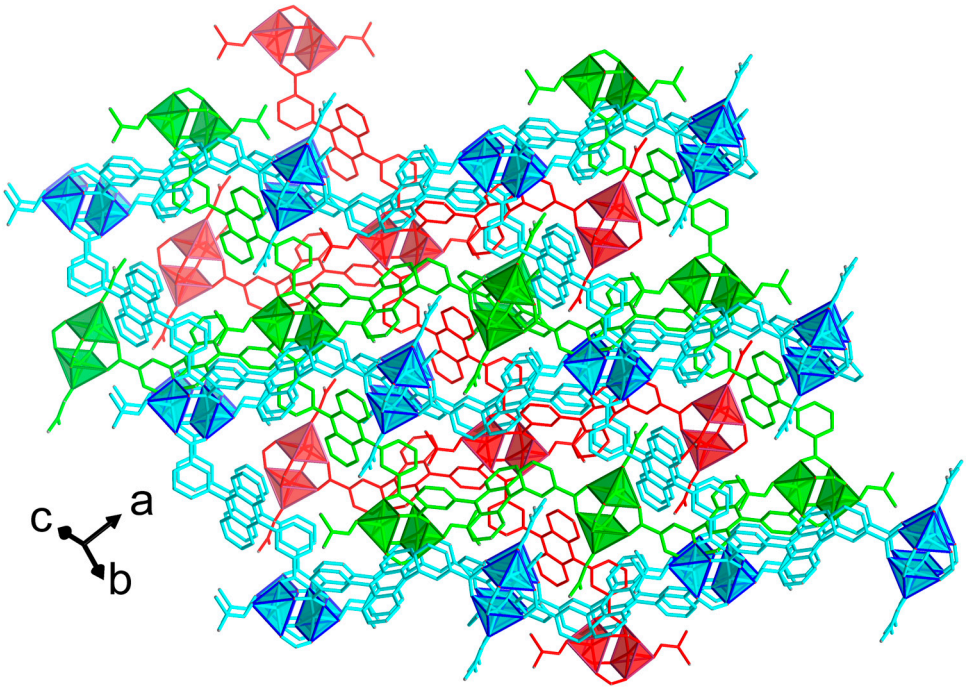

(**a**)

Figure 3. *Cont.*

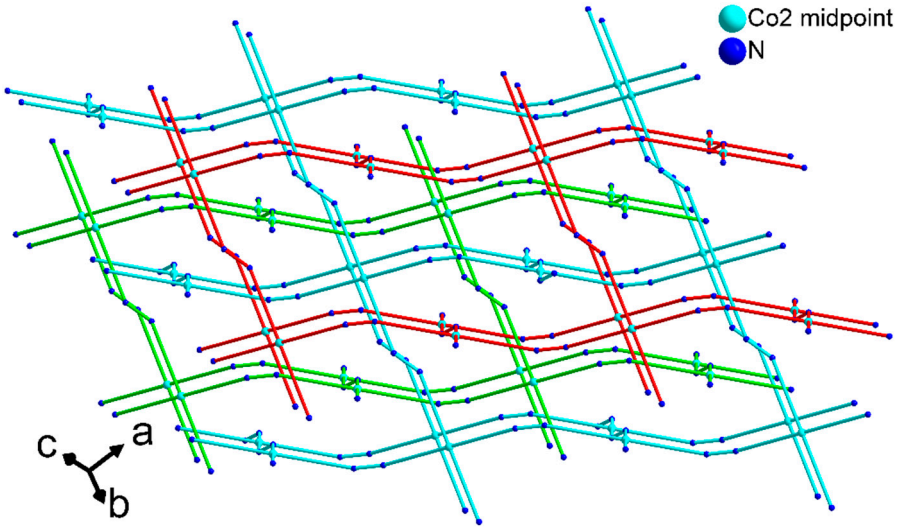

(**b**)

Figure 3. (**a**) The threefold interpenetrated structure of [Co(pdb)(DMF)]. Each network is shown in a different color. (**b**) Schematic representation of the threefold interpenetrated cds net in [Co(pdb)(DMF)], taking the midpoint of the Co_2 handle as a fourfold node. The rods connect the Co_2 midpoints and the phenazine-ring nitrogen atoms.

The combined TGA-DTG curve of [Co(pdb)(DMF)] is shown in Figure S18, and the TG-MS (TGA coupled with mass spectrometry) measurement is shown in Figure S20. The sample was pre-dried for 14 h at 180 °C under vacuum, cooled down under vacuum and rapidly transferred to the TGA instrument. There is no detectable mass loss below approximately 300 °C. The first mass-loss event of about 13 wt% is evident in the DTG at 360 °C and assigned to the removal of the DMF ligand (theor. 13 wt%) The solvent removal transits into the network decomposition of [Co(pdb)] without a clear plateau, and the sample is completely decomposed at ~430 °C with a concomitant mass loss of 73 wt% (theor. 76 wt%), as corroborated by the pronounced DTG minimum at around 410 °C. The final residue remains unchanged at approximately 14–15 wt%, consistent with the formation of cobalt oxide (CoO; theor. 14 wt% for CoO, 15 wt% for Co_2O_3, and 11 wt% for Co).

3.2. Crystal Structure of [Co_2(pdi)(DMF)$_3$]·2(DMF)·H_2O

Figure 4 depicts the extended asymmetric unit and cobalt coordination environment of [Co_2(pdi)(DMF)$_3$]·2(DMF)·H_2O, and Table 1 gives the crystallographic data. The space group of this compound is $Pna2_1$ in the orthorhombic crystal system. The asymmetric unit contains two crystallographically different cobalt(II) ions, a full pdi linker, three coordinated DMF ligands, two non-coordinated DMF molecules and a water molecule of solvation. Both cobalt(II) ions are sixfold coordinated and surrounded by six oxygen atoms, and they, again, form a Co_2 handle as the secondary building unit. The Co1 ion is coordinated by the three DMF ligands and three carboxyl oxygen atoms of three different linkers in the facial configuration. Co2 is coordinated by four different pdi linkers, with two of them chelating and two monodentate. Each of the bridging linkers is connected to Co2, which can be seen as the primary metal node. Out of the four different carboxyl groups of the linker, two are monodentate bridging (O1-C-O2, O3-C-O4) between the two Co ions; one is bidentate bridging between Co1 and Co2 and, at the same time, chelating to Co2 (O5-C-O6 as κO:κO,κO'); and the last one is bidentate chelating to Co2 (O7-C-O8). From the perspective of the linker, each pdi ligand is bound to seven cobalt atoms, i.e., acts as a heptadentate-bridging ligand and connects four Co_2 handles. Three handles are connected

to both cobalt atoms—one handle only through one Co atom. Selected bond lengths and angles are listed in Table 3.

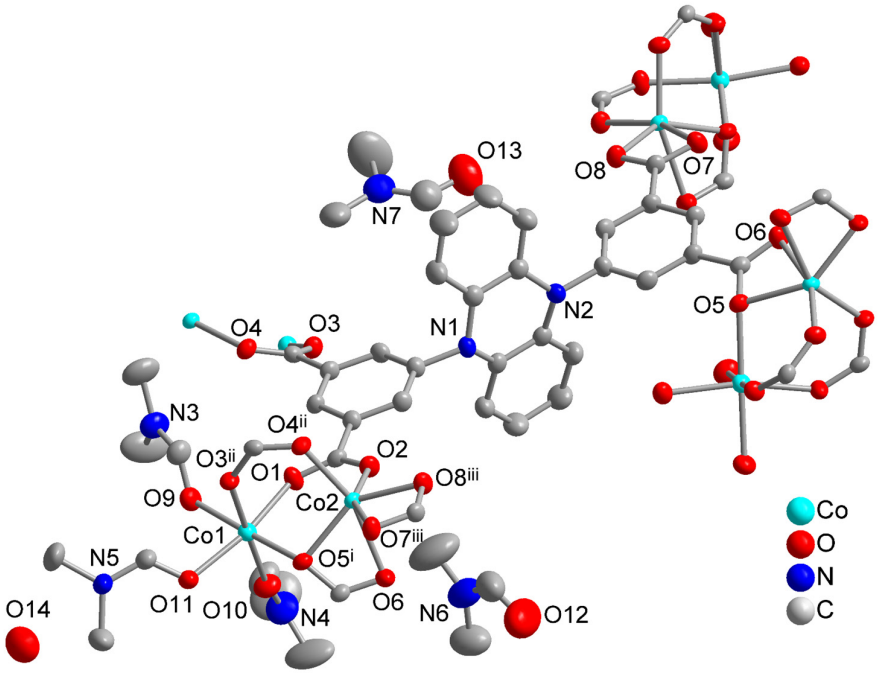

Figure 4. Expanded asymmetric unit for $[Co_2(pdi)(DMF)_3]\cdot 2(DMF)\cdot H_2O$. Symmetry code: (i) −x + 1/2, −y + 3/2, −z + 3/2; (ii) −x + 3/2, y, −z + 1; (iii) −x, −y + 1, −z + 1 (50% thermal ellipsoids). Hydrogen atoms are not shown for clarity.

Table 3. Selected bond lengths (Å) and angles (°) for $[Co_2(pdi)(DMF)_3]\cdot 2(DMF)\cdot H_2O$ [(a)].

Interaction	Bond Length [Å]	Interaction	Angles [°]
Co1—O1	2.072 (3)	O10—Co1—O5 [i]	91.01 (16)
Co1—O3 [ii]	2.040 (3)	O10—Co1—O11	91.32 (16)
Co1—O5 [i]	2.105 (3)	O10—Co1—O1	89.36 (16)
Co1—O9	2.128 (4)	O10—Co1—O9	91.85 (17)
Co1—O10	2.069 (4)	O11—Co1—O5 [i]	93.69 (14)
Co1—O11	2.097 (3)	O11—Co1—O9	86.46 (15)
Co2—O2	1.993 (3)		
Co2—O4 [ii]	2.037 (3)	O2—Co2—O5 [i]	106.59 (15)
Co2—O5 [i]	2.105 (3)	O2—Co2—O4 [ii]	94.93 (15)
Co2—O6 [i]	2.270 (4)	O2—Co2—O7 [iii]	153.89 (13)
Co2—O7 [iii]	2.265 (4)	O2—Co2—O8 [iii]	93.13 (14)
Co2—O8 [iii]	2.050 (3)	O2—Co2—O6 [i]	94.23 (15)
O1—Co1—O5 [i]	97.97 (13)	O4 [ii]—Co2—O5 [i] O4 [ii]—Co2—O7 [iii]	100.40 (13) 95.87 (14)
O1—Co1—O11	168.31 (14)	O4 [ii]—Co2—O8 [iii]	108.82 (15)

Table 3. *Cont.*

Interaction	Bond Length [Å]	Interaction	Angles [°]
O1—Co1—O9	81.86 (14)	O4 ^{ii}—Co2—O6 ^{i}	160.17 (13)
O3 ^{ii}—Co1—O5 ^{i}	86.19 (14)	O5 ^{i}—Co2—O7 ^{iii}	94.72 (13)
O3 ^{ii}—Co1—O11	88.10 (15)	O5 ^{i}—Co2—O6 ^{i}	60.06 (12)
O3 ^{ii}—Co1—O1	91.80 (15)	O8 ^{iii}—Co2—O5 ^{i}	143.07 (13)
O3 ^{ii}—Co1—O9	90.95 (15)	O8 ^{iii}—Co2—O7 ^{iii}	60.87 (13)
O3 ^{ii}—Co1—O10	177.10 (16)	O8 ^{iii}—Co2—O6 ^{i}	88.18 (14)
Co1—Co2	3.368 (1)	Co2 ^{iv}—O5—Co1 ^{iv}	106.27 (14)

(a) Symmetry code: i = −x + 1/2, −y + 3/2, −z + 3/2; ii = −x + 3/2, y, −z + 1; iii = −x, −y + 1, −z + 1; iv = x + 1/2, −y + 3/2, z.

In $[Co_2(pdi)(DMF)_3]\cdot 2(DMF)\cdot H_2O$, crystal water and non-coordinated DMF solvent molecules are incorporated by hydrogen bonds in the crystal lattice. The hydrogen bonds of the crystal water molecule are shown in Figure 5. Hydrogen bond O14–H14A···O8^{ii} is between the water molecule and a cobalt-coordinating carboxyl oxygen atom of the pdi linker, and hydrogen bond O14–H14B···O13^{ii} is a bridge to a non-coordinated DMF molecule. These two hydrogen bonds are of medium strength, as the distance between the hydrogen atom and the accepting oxygen atom is between 1.9 and 2.0 Å in both cases. There is no π–π interaction—only C-H···π interactions originating from a coordinated DMF molecule in the packing of $[Co_2(pdi)(DMF)_3]\cdot 2(DMF)\cdot H_2O$. Also, the C–H···O interactions are largely between DMF molecules or from a coordinated DMF-CHO group to a cis-O atom of a carboxylate group. The water molecule accepts C-H bonds from DMF-CH_3 and a diisophthalate-CH (see Section S9 for details).

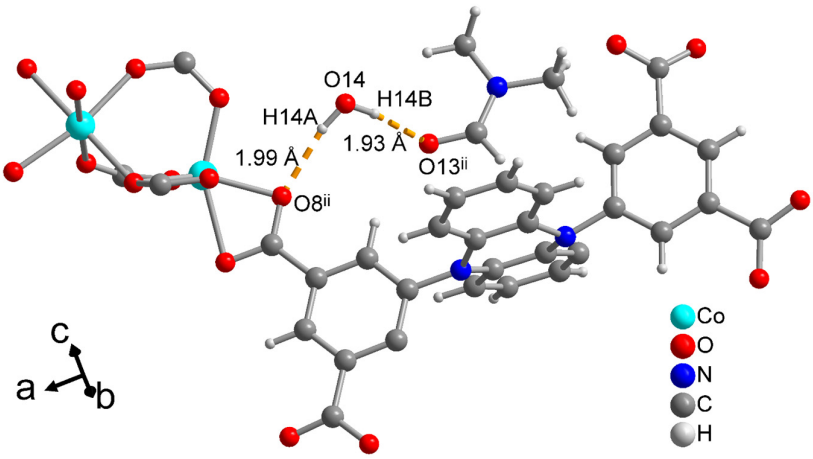

Figure 5. Hydrogen bonds (orange dotted lines) from the crystal water molecule in $[Co_2(pdi)(DMF)_3]\cdot 2(DMF)\cdot H_2O$.

The Co-pdi bridging action gives rise to a three-dimensional network (Figure 6). In this metal–ligand 3D network, there would be open channels (Figure 6a), which are, however, occupied by the coordinated DMF ligands, together with the DMF and H_2O solvent molecules of crystallization (Figure 6b). When the free solvent molecules are omitted in the network, only small voids remain (Figure 7).

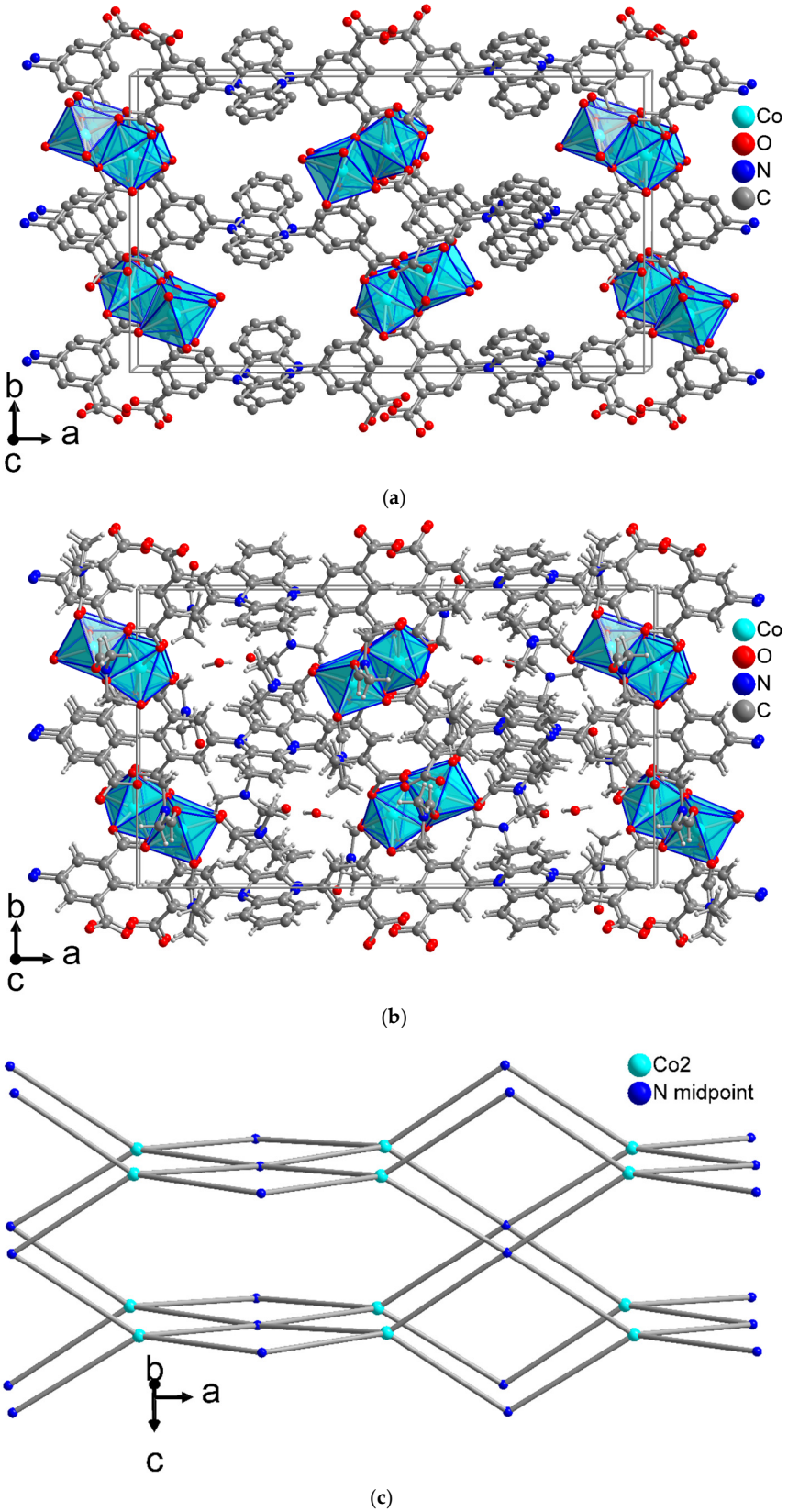

Figure 6. 3D network of $[Co_2(pdi)(DMF)_3]\cdot 2(DMF)\cdot H_2O$. (**a**) Hydrogen atoms, all DMF molecules and H_2O molecules are omitted for clarity. (**b**) Hydrogen atoms, all DMF molecules and H_2O molecules are shown within the unit cell. (**c**) Schematic representation of the pts net in $[Co_2(pdi)(DMF)_3]$, taking the Co2 atom and the linker as fourfold nodes. The rods connect the Co2 atom and the midpoint of the phenazine-ring nitrogen atoms.

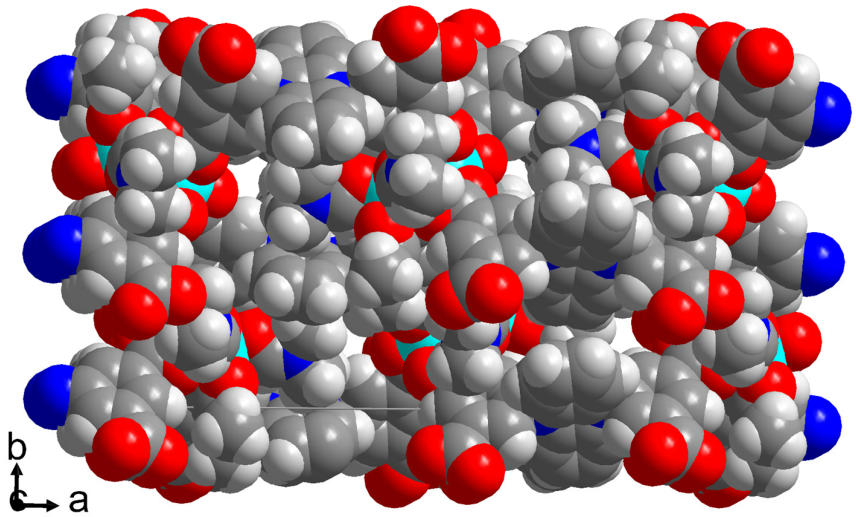

Figure 7. Space-filling view of the network $[Co_2(pdi)(DMF)_3]$ with the coordinated DMF ligands to illustrate remaining small voids when the DMF and H_2O solvent of crystallization were omitted (Co = cyan, O = red, N = blue, C = grey, H = white).

After activation, no N_2 gas uptake could be detected with a volumetric gas sorption analyzer; hence, there is no N_2 accessible porosity in the $[Co_2(pdi)(DMF)_3]$ network. In view of the tight framework packing, the removal of the free DMF was probably not fully achieved, the framework partially collapsed and the potential voids were too small. For sorption measurement, the samples were pre-dried for 12 h at 60 °C under vacuum, then activated at the sorption analyzer under turbomolecular pump vacuum ($5 \cdot 10^{-12}$ bar) for 3 h at 130 °C, as stated in Section 2. The PXRD of the activated $[Co_2(pdi)(DMF)_3]\cdot 2(DMF)\cdot H_2O$ sample shown in Figure S16 indicates that under these conditions, the sample turned amorphous, losing its defined pore structure.

The network topology in $[Co_2(pdi)(DMF)_3]$ is pts (or platinum(II) sulfide) [37,47–49] when taking the Co2 atom as a tetrahedral and the linker as a square–planar fourfold node (Figure 6c). Among the two Co atoms, only Co2 is connected to each of the four carboxyl groups of the linker and is responsible for 3D network formation. Compared to the PtS structure, which is composed of square–planar Pt(II) and tetrahedral sulfide atoms, the pts topology in $[Co_2(pdi)(DMF)_3]$ is reversed such that the metal node is tetrahedral and the linker square–planar.

For thermogravimetric analysis, the sample was pre-dried for 14 h at 180 °C under vacuum, cooled down under vacuum and rapidly transferred to the TGA instrument. The crystal solvent molecules water and DMF were removed under these conditions. The combined TGA–DTG curve (Figure S19) shows the first mass loss at ~300 °C due to the loss of the coordinated DMF (theor. 26 wt%). Without a pronounced plateau, the mass loss continues to ~390 °C with degradation of the organic linker (theor. 60 wt%). At 1000 °C, a residue of 21 wt% remains (theor. 18 wt% for CoO, 20 wt% for Co_2O_3, and 14 wt% for Co).

A comparison of the coordination polymer [Co(pdb)(DMF)] with the structurally related coordination polymers derived from isomeric dihydrophenazine-based dicarboxylate ligand H_2PZDB (Figure 8) [29] highlights the combined influence of metal coordination preferences and ligand geometry on framework assembly. Although the two ligands share the same dihydrophenazine core, the relative orientation of the carboxylate groups differs between the meta and para positions, resulting in different coordination modes and network topologies. In the zinc and cobalt(II) coordination polymers based on H_2PZDB [29], the axial or linear para-arrangement of the carboxylate functions favors extended but less densely interconnected networks, which predominantly adopt lower-dimensional

architectures. In contrast, the pdb ligand employed in this work enforces a more angular coordination geometry through the meta-positions of the carboxylate groups, enabling tetradentate binding to dinuclear cobalt paddle-wheel units, and promotes the formation of a fully three-dimensional cds net with pronounced interpenetration.

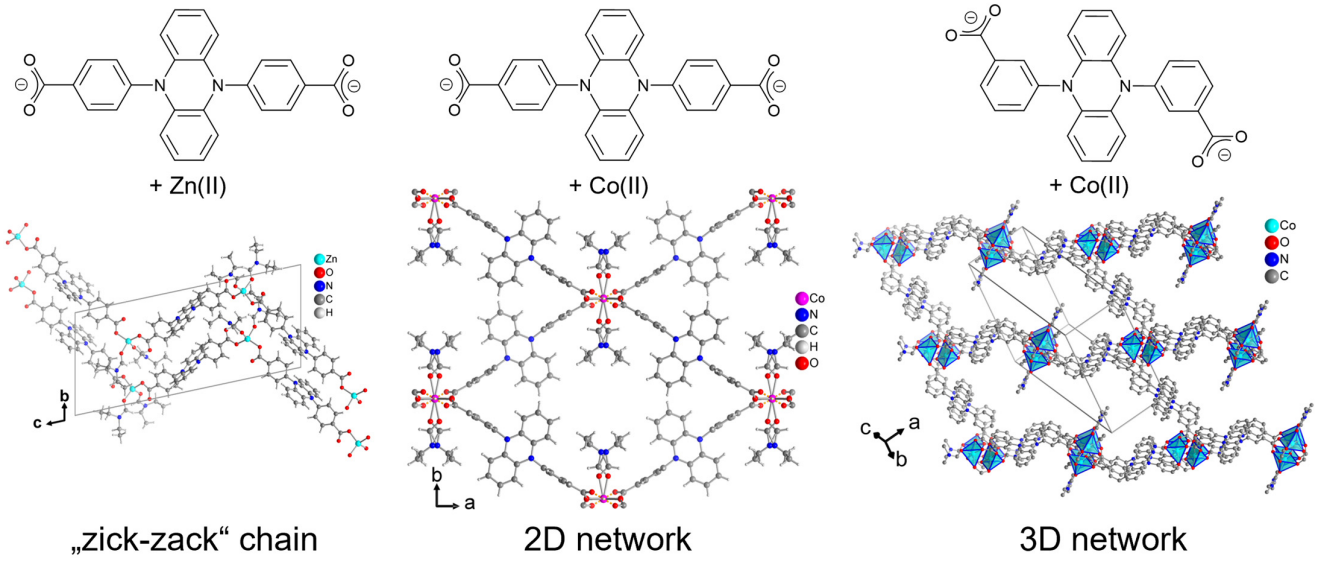

Figure 8. Simplified structural comparison of dihydrophenazine-based coordination polymers, highlighting the influence of ligand geometry and metal coordination on network topology. Coordination polymers based on isomeric dicarboxylate ligand H_2PZDB (**left** and **center**; adapted from Reference [29]) form less densely interconnected architectures, whereas the cobalt(II) coordination polymer [Co(pdb)(DMF)] reported in this work (**right**) adopts a three-dimensional, highly interpenetrated framework. The comparison illustrates how subtle changes in carboxylate connectivity, in combination with the coordination flexibility of cobalt(II), govern framework dimensionality and packing.

Cyclovoltammetric (CV) studies were performed to investigate the redox behavior of phenazine-containing cobalt coordination compounds. However, [Co(pdb)(DMF)] exhibits only limited electrochemical stability under the applied conditions, as evidenced by the progressive changes in the cyclovoltammograms upon repeated cycling. In particular, continuous decrease and distortion of the redox features are observed (Figure S27a), indicating irreversible processes and/or decomposition of the electroactive species. For $[Co_2(pdi)(DMF)_3]\cdot 2(DMF)\cdot H_2O$, no well-defined redox waves could be obtained within the accessible potential window (Figure S27b). The recorded currents are largely featureless and dominated by background processes, suggesting that the redox events of the compound are either electrochemically irreversible or masked by concurrent chemical reactions. Consequently, CV measurements were not further used for quantitative analysis of the redox properties but are provided here only to document the observed behavior.

4. Conclusions

Two cobalt(II) coordination networks based on dihydrophenazine-derived dicarboxylate and tetracarboxylate linkers H_2pdb and H_4pdi were synthesized solvothermally and structurally characterized. Crystalline products were obtained only with cobalt(II) nitrate, highlighting the sensitivity of framework formation to the metal ion and its counterion when using rigid, multitopic carboxylate linkers. Systematic solvothermal reactions with other metal salts (Zr(IV), Al(III), Cu(II), Ni(II), and Zn(II)) under comparable conditions resulted in no or non-crystalline products. Only cobalt(II) nitrate yielded single crystals

suitable for X-ray diffraction; notably, analogous reactions with cobalt(II) sulfate or chloride were unsuccessful, indicating a pronounced counterion effect.

In [Co(pdb)(DMF)], dinuclear cobalt paddle-wheel units are linked by tetradentate pdb ligands into a three-dimensional cds net that exhibits threefold interpenetration and results in a densely packed framework. In contrast, $[Co_2(pdi)(DMF)_3]\cdot 2(DMF)\cdot H_2O$ contains two crystallographically distinct cobalt(II) centers, of which only one propagates the three-dimensional network, giving rise to an inverse pts topology with tetrahedral metal nodes and square–planar linker nodes.

These compounds demonstrate how the connectivity and geometry of dihydrophenazine-based carboxylate ligands govern the formation of secondary building units, network topology, and interpenetration in cobalt coordination polymers.

Supplementary Materials: The following supporting information can be downloaded at: https://www.mdpi.com/article/10.3390/cryst16030185/s1, Section S1: Chemicals used; Section S2: Reaction schemes for ligand syntheses; Section S3: NMR spectra; Section S4: IR spectra; Section S5: Overview of the conducted studies; Section S6: Crystal photographs and crystal structure images; Section S7: PXRD; Section S8: Thermogravimetric analyses; Section S9: Supramolecular analyses; Section S10: Electrochemical measurements. References [20,50–55] are cited in the Supplementary Materials.

Author Contributions: Conceptualization, A.V. and C.J.; methodology, A.V.; software, A.V.; validation, A.V., X.L. and N.J.; formal analysis, A.V., X.L., N.J., P.S. and D.G.; investigation, A.V., X.L., N.J., P.S. and D.G.; resources, C.J.; data curation, A.V., X.L. and N.J.; writing—original draft preparation, A.V. and C.J.; writing—review and editing, A.V. and C.J.; visualization, A.V. and C.J.; supervision, C.J.; project administration, C.J.; funding acquisition, C.J. All authors have read and agreed to the published version of the manuscript.

Funding: Funding was provided by the Deutsche Forschungsgemeinschaft (DFG) under grant 440366605 (for the Rigaku diffractometer). This work was supported by the Deutsche Forschungsgemeinschaft (DFG, German Research Foundation)—396890929/GRK 2482.

Data Availability Statement: The data presented in this study are available upon request from the corresponding author. The CCDC numbers 2522790–2522791 for compounds [Co(pdb)(DMF)] and $[Co_2(pdi)(DMF)_3]\cdot 2(DMF)\cdot H_2O$, respectively, contain the supplementary crystallographic data reported in this paper. These data can be obtained free of charge from the Cambridge Crystallographic Data Center via www.ccdc.cam.ac.uk/data_request/cif (accessed on 14 January 2026).

Acknowledgments: The authors would like to thank Birgit Tommes for providing the IR measurements. We also thank the Center for Molecular and Structural Analytics at Heinrich Heine University (CeMSA@HHU) for recording the mass spectrometric and NMR spectrometric data.

Conflicts of Interest: The authors declare no conflicts of interest.

References

1. Feng, S.; Wang, L.; Tian, L.; Liu, Y.; Hu, K.; Xu, H.; Wang, H.; Hua, J. Leveraging phenazine and dihydrophenazine redox dynamics in conjugated microporous polymers for high-efficiency overall photosynthesis of hydrogen peroxide. *Chem. Sci.* **2024**, *15*, 11972–11980. [CrossRef] [PubMed]
2. Ding, B.; Solomon, M.B.; Leong, C.F.; D'Alessandro, D.M. Redox-active ligands: Recent advances towards their incorporation into coordination polymers and metal-organic frameworks. *Coord. Chem. Rev.* **2021**, *439*, 213891. [CrossRef]
3. Liao, P.-Q.; Shen, J.-Q.; Zhang, J.-P. Metal–organic frameworks for electrocatalysis. *Coord. Chem. Rev.* **2018**, *373*, 22–48. [CrossRef]
4. D'Alessandro, D.M. Exploiting redox activity in metal–organic frameworks: Concepts, trends and perspectives. *Chem. Commun.* **2016**, *52*, 8957–8971. [CrossRef]
5. Lee, J.; Shizu, K.; Tanaka, H.; Nakanotani, H.; Yasuda, T.; Kaji, H.; Adachi, C. Controlled emission colors and singlet–triplet energy gaps of dihydrophenazine-based thermally activated delayed fluorescence emitters. *J. Mater. Chem. C* **2015**, *3*, 2175–2181. [CrossRef]

6. Dulov, D.A.; Bogdanov, A.V.; Dorofeev, S.G.; Magdesieva, T.V. *N*,*N*-Diaryldihydrophenazines as a Sustainable and Cost-Effective Alternative to Precious Metal Complexes in the PhotoredoxCatalyzed Alkylation of Aryl Alkyl Ketones. *Molecules* **2023**, *28*, 221. [CrossRef]
7. Corbin, D.A.; McCarthy, B.G.; van de Lindt, Z.; Miyake, G.M. Radical Cations of Phenoxazine and Dihydrophenazine Photoredox Catalysts and Their Role as Deactivators in Organocatalyzed Atom Transfer Radical Polymerization. *Macromolecules* **2021**, *54*, 4726–4738. [CrossRef]
8. Suzuki, S.; Takeda, T.; Kuratsu, M.; Kozaki, M.; Sato, K.; Shiomi, D.; Takui, T.; Okada, K. Pyrene-dihydrophenazine bis(radical cation) in a singlet ground state. *Org. Lett.* **2009**, *11*, 2816–2818. [CrossRef]
9. Unglaube, F.; Hünemörder, P.; Guo, X.; Chen, Z.; Wang, D.; Mejía, E. Phenazine Radical Cations as Efficient Homogeneous and Heterogeneous Catalysts for the Cross-Dehydrogenative Aza-Henry Reaction. *Helv. Chim. Acta* **2020**, *103*, e2000184. [CrossRef]
10. Lin, J.; Ouyang, J.; Liu, T.; Li, F.; Sung, H.H.-Y.M.; Williams, I.; Quan, Y. Metal-organic framework boosts heterogeneous electron donor–acceptor catalysis. *Nat. Commun.* **2023**, *14*, 7757. [CrossRef]
11. Hong, Q.-Y.; Huang, B.; Wu, M.-X.; Xu, L.; Zhao, X.-L.; Shi, X.; Yang, H.-B. Redox-Active Dihydrophenazine-Based Macrocycle: Synthesis, Conformation-Adaptive Behavior and Host-Guest Complexation with Tetracyanoquinodimethane. *Chin. J. Chem.* **2024**, *42*, 1895–1900. [CrossRef]
12. Theriot, J.C.; Lim, C.-H.; Yang, H.; Ryan, M.D.; Musgrave, C.B.; Miyake, G.M. Organocatalyzed atom transfer radical polymerization driven by visible light. *Science* **2016**, *352*, 1082–1086. [CrossRef] [PubMed]
13. Cheng, Y.; Li, Y.-X.; Liu, C.-H.; Zhu, Y.-Y.; Lin, W. Diaryl Dihydrophenazine-Based Porous Organic Polymers Enhance Synergistic Catalysis in Visible-Light-Driven Organic Transformations. *Angew. Chem. Int. Ed.* **2023**, *62*, e202310470. [CrossRef]
14. Corbin, D.A.; Puffer, K.O.; Chism, K.A.; Cole, J.P.; Theriot, J.C.; McCarthy, B.G.; Buss, B.L.; Lim, C.-H.; Lincoln, S.R.; Newell, B.S.; et al. Radical Addition to *N*,*N*-Diaryl Dihydrophenazine Photoredox Catalysts and Implications in Photoinduced Organocatalyzed Atom Transfer Radical Polymerization. *Macromolecules* **2021**, *54*, 4507–4516. [CrossRef] [PubMed]
15. Cole, J.P.; Federico, C.R.; Lim, C.-H.; Miyake, G.M. Photoinduced organocatalyzed atom transfer radical polymerization using low ppm catalyst loading. *Macromolecules* **2019**, *52*, 747–754. [CrossRef]
16. Su, X.; Jessop, P.G.; Cunningham, M.F. Versatility of organocatalyzed atom transfer radical polymerization and CO_2-switching for preparing both hydrophobic and hydrophilic polymers with the recycling of a photocatalyst. *Macromolecules* **2019**, *52*, 6725–6733. [CrossRef]
17. McCarthy, B.; Sartor, S.; Cole, J.; Damrauer, N.; Miyake, G.M. Solvent effects and side reactions in organocatalyzed atom transfer radical polymerization for enabling the controlled polymerization of acrylates catalyzed by diaryl dihydrophenazines. *Macromolecules* **2020**, *53*, 9208–9219. [CrossRef]
18. Wang, K.; Kang, X.; Yuan, C.; Han, X.; Liu, Y.; Cui, Y. Porous 2D and 3D Covalent Organic Frameworks with Dimensionality-Dependent Photocatalytic Activity in Promoting Radical Ring-Opening Polymerization. *Angew. Chem. Int. Ed.* **2021**, *60*, 19466–19476. [CrossRef]
19. Kochetygov, I.; Roth, J.; Espín, J.; Pache, S.; Justin, A.; Schertenleib, T.; Taheri, N.; Chernyshov, D.; Queen, W.L. A Simple, Transition Metal Catalyst-Free Method for the Design of Complex Organic Building Blocks Used to Construct Porous Metal-Organic-Frameworks. *Angew. Chem. Int. Ed.* **2023**, *62*, e202215595. [CrossRef]
20. Zhang, S.; Ma, X.-F.; Yang, Y.; Ren, H.; Li, W.; Liu, Y.; Xi, C.; Zheng, L.; Miao, Z. Phenazine-functionalized Zn-based metal organic framework for efficient visible light photocatalytic sulfides. *J. Solid State Chem.* **2025**, *351*, 125525. [CrossRef]
21. Jiang, W.L.; Huang, B.; Zhao, X.L.; Shi, X.; Yang, H.B. Strong halide anion binding within the cavity of a conformation-adaptive phenazine-based Pd_2L_4 cage. *Chem* **2023**, *9*, 2655–2668. [CrossRef]
22. Zhang, H.; Tanga, X.; Gu, C. Dihydrophenazine linked porous organic polymers for high capacitance and energy density pseudocapacitive electrodes and devices. *J. Mater. Chem. A* **2021**, *9*, 4984–4989. [CrossRef]
23. Vitaku, E.; Gannett, C.N.; Carpenter, K.L.; Shen, L.; Abruna, H.D.; Dichtel, W.R. Phenazine-Based Covalent Organic Framework Cathode Materials with High Energy and Power Densities. *J. Am. Chem. Soc.* **2020**, *142*, 16–20. [CrossRef] [PubMed]
24. Wu, M.-X.; Hong, Q.-Y.; Li, M.; Jiang, W.-L.; Huang, B.; Lu, S.; Wang, H.; Yang, H.-B.; Zhao, X.-L.; Shi, X. Self-assembly of conformation-adaptive dihydrophenazine-based coordination cages. *Chem. Commun.* **2024**, *60*, 1184–1187. [CrossRef]
25. Yu, J.; Cheng, L.; Zhang, X.; Shi, X.; Wang, H.-g. Integrating p-type phenazine into covalent triazine framework to achieve co-storage of cations and anions for quasi-solid-state dual-ion batteries. *Chem. Eng. J.* **2024**, *489*, 151320. [CrossRef]
26. Guo, J.; Xu, Y.; Jin, S.; Chen, L.; Kaji, T.; Honsho, Y.; Addicoat, M.A.; Kim, J.; Saeki, A.; Ihee, H.; et al. Conjugated organic framework with three-dimensionally ordered stable structure and delocalized π clouds. *Nat. Commun.* **2013**, *4*, 2736. [CrossRef]
27. Sun, H.; Ji, H.; Qiao, D.; Xu, Y.; Qu, X.; Qi, Y.; Feng, Z.; Zhang, X.; Zhang, F.; Wang, R.; et al. Vinylene-linked covalent organic frameworks based on phenanthroline for visible-light-driven bifunctional photocatalytic water splitting. *Chem. Eng. J.* **2025**, *507*, 160448. [CrossRef]
28. Jiang, W.-L.; Huang, B.; Wu, M.-X.; Zhu, Y.-K.; Zhao, X.-L.; Shi, X.; Yang, H.-B. Post-Synthetic Modification of Metal-Organic Frameworks Bearing Phenazine Radical Cations for aza-Diels-Alder Reactions. *Chem. Asian J.* **2021**, *16*, 3985–3992. [CrossRef]

29. Püschel, D.; Nau, M.; Assahub, N.; Beglau, T.H.Y.; Hufnagel, N.; Jordan, D.; Heinen, T.; Strothmann, T.; Suta, M.; Winter, R.F.; et al. Zinc and Cobalt Coordination Polymers Based on the Redox-Active Linker 4,4′-(Phenazine-5,10-diyl)dibenzoate: Structures and Electrochemical Properties. *Eur. J. Inorg. Chem.* **2025**, *28*, e202500270. [CrossRef]
30. Dolomanov, O.V.; Bourhis, L.J.; Gildea, R.J.; Howard, J.A.K.; Puschmann, H. OLEX2: A complete structure solution, refinement and analysis program. *J. Appl. Crystallogr.* **2009**, *42*, 339–341. [CrossRef]
31. Sheldrick, G.M. SHELXT—Integrated space-group and crystal-structure determination. *Acta Crystallogr. A* **2015**, *71*, 3–8. [CrossRef] [PubMed]
32. Sheldrick, G.M. Crystal structure refinement with SHELXL. *Acta Crystallogr. C* **2015**, *71*, 3–8. [CrossRef] [PubMed]
33. Brandenburg, K. *Diamond*; Version 5.0.0; Crystal and Molecular Structure Visualization, Crystal Impact; K. Brandenburg & H. Putz Gbr: Bonn, Germany, 1997–2023.
34. Macrae, C.F.; Sovago, I.; Cottrell, S.J.; Galek, P.T.A.; McCabe, P.; Pidcock, E.; Platings, M.; Shields, G.P.; Stevens, J.S.; Towler, M.; et al. Mercury 4.0: From visualization to analysis, design and prediction. *J. Appl. Crystallogr.* **2020**, *53*, 226–235. [CrossRef] [PubMed]
35. Dai, G.; He, Y.; Niu, Z.; He, P.; Zhang, C.; Zhao, Y.; Zhang, X.; Zhou, H. A Dual-Ion Organic Symmetric Battery Constructed from Phenazine-Based Artificial Bipolar Molecules. *Angew. Chem. Int. Ed.* **2019**, *58*, 9902–9906. [CrossRef]
36. Koyama, D.; Dale, H.J.A.; Orr-Ewing, A.J. Ultrafast Observation of a Photoredox Reaction Mechanism: Photoinitiation in Organocatalyzed Atom-Transfer Radical Polymerization. *J. Am. Chem. Soc.* **2018**, *140*, 1285–1293. [CrossRef]
37. Delgado-Friedrichs, O.; O'Keeffe, M.; Yaghi, O.M. Three-periodic nets and tilings: Edge-transitive binodal structures. *Acta Crystallogr. A* **2006**, *62*, 350–355. [CrossRef]
38. Friedrichs, O.D.; O'Keeffe, M.; Yaghi, O.M. The $CdSO_4$, rutile, cooperite and quartz dual nets: Interpenetration and catenation. *Solid State Sci.* **2003**, *5*, 73–78. [CrossRef]
39. Friedrichs, O.D.; O'Keeffe, M. Three-periodic tilings and nets: Face-transitive tilings and edge-transitive nets revisited. *Acta Crystallogr. A* **2007**, *63*, 344–347. [CrossRef]
40. Moulton, B.; Abourahma, H.; Bradner, M.W.; Lu, J.; McManus, G.J.; Zaworotko, M.J. A new $6^5.8$ topology and a distorted $6^5.8$ $CdSO_4$ topology: Two new supramolecular isomers of $[M_2(bdc)_2(L)_2]_n$ coordination polymers. *Chem. Commun.* **2003**, 1342–1343. [CrossRef]
41. Gao, H.; Lou, X.H.; Li, Q.T.; Du, W.J.; Xu, C. Three-Fold Interpenetrated $CdSO_4$ Topology in a Co(II) Coordination Polymer Constructed From Pamoic Acid and N-Containing Auxiliary Ligand. *Synth. React. Inorg. Met.-Org. Nano-Met. Chem.* **2015**, *45*, 865–868. [CrossRef]
42. Zhang, J.; Chen, Y.-B.; Ji, Z.; Qin, Y.-Y.; Yao, Y.-G. A rare twofold interpenetrated cds topology in a Zn-organic polymer $[Zn_2(BDC)(BPP)Cl_2]_n$. *Inorg. Chem. Commun.* **2006**, *9*, 449–451. [CrossRef]
43. Gaskin, G.J.; LaDuca, R.L. Poly[[[μ-1,4-bis(pyridin-4-ylmethyl)piperazine][μ-4-(2-carboxylatoethyl)benzoato]copper(II)] monohydrate], a coordination polymer with twofold interpenetrated cds topology networks. *IUCrData* **2023**, *8*, x230855. [CrossRef] [PubMed]
44. Tsai, M.-J.; Liao, K.-S.; Wu, J.-Y. A Water-Stable 2-Fold Interpenetrating cds Net as a Bifunctional Fluorescence-Responsive Sensor for Selective Detection of Cr(III) and Cr(VI) Ions. *Nanomaterials* **2022**, *12*, 158. [CrossRef] [PubMed]
45. Kostakis, G.E.; Casella, L.; Hadjiliadis, N.; Monzani, E.; Kourkoumelis, N.; Plakatouras, J.C. Interpenetrated networks from a novel nanometer-sized pseudopeptidic ligand, bridging water, and transition metal ions with cds topology. *Chem. Commun.* **2005**, 3859–3861. [CrossRef]
46. Shi, Z.-C.; Wang, X.; Drozd, V.; Raptis, R.G. A Foldable Metal–Organic Framework with cds Topology Assembled via Four-Connected Square-Planar Single Ni^{2+}-Ion Nodes and Linear Bidentate Linkers. *Crystals* **2024**, *14*, 40. [CrossRef]
47. Zhang, J.; Xue, Y.-S.; Liang, L.-L.; Ren, S.-B.; Li, Y.-Z.; Du, H.-B.; You, X.-Z. Porous Coordination Polymers of Transition Metal Sulfides with PtS Topology Built on a Semirigid Tetrahedral Linker. *Inorg. Chem.* **2010**, *49*, 7685–7691. [CrossRef]
48. Yuan, A.-H.; Lu, R.-Q.; Zhou, H.; Chen, Y.-Y.; Li, Y.-Z. Three unique two-fold interpenetrated three-dimensional networks with PtS-type topology constructed from $[M(CN)_4]^{2-}$ (M = Ni, Pd, Pt) as "square-planar" building blocks. *CrystEngComm* **2010**, *12*, 1382–1384. [CrossRef]
49. Murphy, M.J.; D'Alessandro, D.M.; Kepert, C.J. A porous Mn(V) coordination framework with PtS topology: Assessment of the influence of a terminal nitride on CO_2 sorption. *Dalton Trans.* **2013**, *42*, 13308–13310. [CrossRef]
50. Mandić, V.; Kurajica, S.; Plodinec, M.; Panžić, I. Thermal Stability and Utilization of 1D-Nanostructured Co_3O_4 Rods Derived by Simple Solvothermal Processing. *Catalysts* **2022**, *12*, 1162. [CrossRef]
51. Spek, A.L. Structure Validation in Chemical Crystallography. *Acta Crystallogr. D* **2009**, *65*, 148–155. [CrossRef]
52. Janiak, C. A Critical Account on π–π Stacking in Metal Complexes with Aromatic Nitrogen-Containing Ligands. *J. Chem. Soc. Dalton Trans.* **2000**, 3885–3896. [CrossRef]

53. Yang, X.-J.; Drepper, F.; Wu, B.; Sun, W.-H.; Haehnel, W.; Janiak, C. From Model Compounds to Protein Binding: Syntheses, Characterizations and Fluorescence Studies of $[Ru^{II}$ (Bipy)(Terpy)L$]^{2+}$ Complexes (Bipy = 2,2′-Bipyridine; Terpy = 2,2′:6′,2″-Terpyridine; L = Imidazole, Pyrazole and Derivatives, Cytochrome c). *Dalton Trans.* **2005**, 256–267. [CrossRef]
54. Takahashi, O.; Kohno, Y.; Iwasaki, S.; Saito, K.; Iwaoka, M.; Tomoda, S.; Umezawa, Y.; Tsuboyama, S.; Nishio, M. Hydrogen-Bond-Like Nature of the CH/π Interaction as Evidenced by Crystallographic Database Analyses and Ab Initio Molecular Orbital Calculations. *Bull. Chem. Soc. Jpn.* **2001**, *74*, 2421–2430. [CrossRef]
55. Nishio, M.; Umezawa, Y.; Honda, K.; Tsuboyama, S.; Suezawa, H. CH/π Hydrogen Bonds in Organic and Organometallic Chemistry. *CrystEngComm* **2009**, *11*, 1757–1788. [CrossRef]